

Disentangling the Link Between Image Statistics and Human Perception

Alexander Hepburn^{1*} Valero Laparra^{2*} Raul Santos-Rodriguez¹ Jesús Malo²

¹ Department of Engineering Mathematics, University of Bristol

²Image Processing Lab, Universitat de Valencia

alex.hepburn@bristol.ac.uk, valero.laparra@uv.es, enrusr@bristol.ac.uk, jesus.malo@uv.es

Abstract

In the 1950s Horace Barlow and Fred Attneave suggested a connection between sensory systems and how they are adapted to the environment: early vision evolved to maximise the information it conveys about incoming signals. Following Shannon’s definition, this information was described using the probability of the images taken from natural scenes. Previously, direct accurate predictions of image probabilities were not possible due to computational limitations. Despite the exploration of this idea being indirect, mainly based on oversimplified models of the image density or on system design methods, these methods had success in reproducing a wide range of physiological and psychophysical phenomena. In this paper, we directly evaluate the probability of natural images and analyse how it may determine perceptual sensitivity. We employ image quality metrics that correlate well with human opinion as a surrogate of human vision, and an advanced generative model to directly estimate the probability. Specifically, we analyse how the sensitivity of full-reference image quality metrics can be predicted from quantities derived directly from the probability distribution of natural images. First, we compute the mutual information between a wide range of probability surrogates and the sensitivity of the metrics and find that the most influential factor is the probability of the noisy image. Then we explore how these probability surrogates can be combined using a simple model to predict the metric sensitivity, giving an upper bound for the correlation of 0.85 between the model predictions and the actual perceptual sensitivity. Finally, we explore how to combine the probability surrogates using simple expressions, and obtain two functional forms (using one or two surrogates) that can be used to predict the sensitivity of the human visual system given a particular pair of images.

1. Introduction

One long standing discussion in artificial and human vision is about the principles that should drive sensory systems. This includes Barlow’s *Efficient Coding Hypothesis* [3, 4], and Marr and Poggio’s functional descriptions at the (more abstract) *Computational Level* of vision [47]. In modern machine learning terms, the above classical ideas connect the probability density function (PDF) of the images with the behaviour of the sensors.

There is an indirect research direction that explores this connection by proposing design principles for the system (such as information maximisation, or factorisation) to find an optimal transformation and compare the features learned by this transformation and the ones found in the visual system (e.g. receptive fields or nonlinearities) [52, 5, 63, 58, 26]. This indirect research direction, which was popular in the past due to limited computational resources, relies on gross approximations of the PDF of natural images and on strong assumptions about the behaviour of the system. Examples of surrogates of the PDF that were proposed as explanations of the behaviour in the above indirect design methods [10, 52, 36, 51, 1, 39, 66, 34, 9] are reviewed below in Section 2.2.

In contrast, here we focus on the functional goal rather than on the system design: we directly relate the behaviour of the system itself (sensitivity) with the PDF of natural images. Following the preliminary suggestions in [24] about this relation we rely on two elements. On the one hand, recent *generative models* that represent large image datasets better than previous PDF approximations and provide us with an accurate estimate of the probability at query points [67, 57]. Whilst these statistical models are not analytical, they allow for sampling and log-likelihood prediction. They also allow us to compute gradients of the probability, which, as reviewed below, have been proven to be related to sensible vision goals.

On the other hand, recent measures of *perceptual distance* between images have recreated human opinion of subjective distortion to a great accuracy [29, 77, 23, 15]. Whilst being just an approximation to human subjectivity, the sen-

*Equal Contributions

sitivity of these perceptual distances is a convenient computational description of the main trends of human vision that should be explained from scene statistics.

In this work, we identify the more relevant probabilistic factors that may be behind the non-Euclidean behavior of perceptual distances and we finally propose a simple expression to predict the sensitivity of the perceptual distances from these factors. First, we empirically show the relationship between the sensitivity of the metrics and probability surrogates using conditional histogram plots. We then compute the mutual information between the sensitivity of the perceptual distances and the probability surrogates. We do it factor-wise and we also consider groups of factors. Then we use different regression models to identify a hierarchy in the factors that allow us to propose analytic relationships for predicting perceptual sensitivity. Finally, we perform analysis over the most simple possible closed-form expressions, and select some solutions to predict the perceptual sensitivity given selected probability surrogates.

2. Background and Proposed Methods

In this section, we first recall the computational description of human behaviour introduced in [24]: the *sensitivity of the perceptual distance*. This subjective sensitivity (which can be computed from the available models of perceptual distance) is the feature to be explained by the probability-related factors considered in this study. Then we review the probability-related factors that have been previously proposed as principles for human vision. Our proposal consists of being able to highlight relations and find explicit expressions to derive behaviour from the statistical factors. Finally, we introduce the tools to compute both behaviour and statistical factors: (i) the perceptual distances, (ii) the probability models, and (iii) how variations in the image space (distorted images) are chosen.

2.1. The problem: Perceptual Sensitivity

Given some original image \mathbf{x} and a distorted version $\tilde{\mathbf{x}}$, full-reference *perceptual distances* are models, $D_p(\mathbf{x}, \tilde{\mathbf{x}})$, that accurately mimic the human opinion about the subjective difference between them. Examples of these models reviewed below include [72, 71, 77, 23, 15].

In general, this perceived distance, $D_p(\mathbf{x}, \tilde{\mathbf{x}})$, is highly dependent on the particular image analysed, i.e. a distance that is independent of the features of the particular image such as the Root Mean Square Error (RMSE), $\|\mathbf{x} - \tilde{\mathbf{x}}\|_2$, does not correlate well with human perception [70]. This dependence on the image is captured by the *sensitivity of the perceptual distance*, defined as [24]:

$$S(\mathbf{x}, \tilde{\mathbf{x}}) = \frac{D_p(\mathbf{x}, \tilde{\mathbf{x}})}{\|\mathbf{x} - \tilde{\mathbf{x}}\|_2} \quad (1)$$

The sensitivity of the perceptual distance, also referred to

as the *perceptual sensitivity* through out the work, relates a (perceptually meaningful) non-Euclidean distance between images with the (perceptually meaningless) Euclidean distance RMSE. This ratio is big at regions of the image space where human sensitivity is high and small at neglected regions. Moreover, this sensitivity is anisotropic: distortions with constant Euclidean length along different directions (distortions of different nature) lead to different subjective distortions and hence sensitivity depends on the direction.

2.2. Probabilistic Explanations of Vision

Following the classical ideas on *efficient coding* and on explanations at the *computational level* mentioned in the introduction, there has been a rich literature explicitly linking specific features of human vision with probabilistic descriptions of the images. Examples of design principles that have been proposed in the past are included in Table 1 together with the associated statistical descriptors.

Principles in Table 1 include: **(i) Information transmission for regular images based on redundancy reduction.** This is at the core of principal component analysis [21, 10], independent components analysis [52, 5, 26] or in PDF equalisation [36] or factorization [45]. In all these cases, the PDF or the loglikelihood are key factors. **(ii) Optimal representations for regular images in presence of noise.** Noise may occur either in the front-end sensors [51, 2, 1] (optimal denoising), or in the internal representation [39, 66] (optimal quantisation, or optimal nonlinearities to cope with noise). While in optimal denoising the solutions depend on the derivative of the loglikelihood [56, 69], optimal discrimination is based on resource allocation according to the PDF after saturating non linearities [66, 40, 59, 18]. Bit allocation and quantization according to nonlinear transforms of the PDF has been used in perceptually optimized image coding [41, 42]. In fact, both factors considered above (the PDF equalisation and the optimal nonlinearities to cope with inner noise) have been unified in a single framework where the representation is driven by the PDF raised to certain exponent [43, 31, 34]. **(iii) Focus on surprising images (as opposed to regular images)** may also drive the sensitivity of the system. This critically different factor (surprise as opposed to regularities) has been pointed out for color perception [19, 76], and in visual saliency [9]. In this case, the surprise is described by the inverse of the probability (as opposed to the probability) as in the core definition of information [60].

The descriptors associated to the above probabilistic explanations have been found to positively (or negatively) correlate to the sensitivity in a number of observations with a restricted set of metrics [24]. However, that study did not consider other statistical descriptors of the signal that have been studied by classical vision science (last three columns of Table 1).

Table 1. Different surrogates of the PDF of natural images (causal factors / explanations) that have been proposed to predict sensitivity.

Information Transmission	Internal Noise	Acquisition Noise	Surprise	Signal Average	Signal Spectrum	Marginal Laplacian
	Limited Resolution	Denoising		First Eigenvalue Mean Luminance	All Eigenvalues Contrast	Marginal nonlinearity
Barlow [4]	Lloyd [39]	Miyasawa [51]	Shannon [60]	Weber [74]	Michelson [50]	Simoncelli [62]
Laughlin [36]	McLeod [40]	Raphan & Simoncelli [56]	Gegenfurtner et al. [19, 76]	Fechner [17]	Campbell & Robson [11]	Heeger [22]
Bell et al. [5]	Twer et al. [66]	Vincent [69]	Bruce & Tsotsos [9]		Peli [53]	Daly [14]
Laparra et al. [32, 34]						Malo et al. [43]
Hepburn et al. [24]						
$p(\mathbf{x})$ $\log(p(\mathbf{x}))$	$p(\mathbf{x})^{\frac{1}{3}}$ $\frac{1}{3}\log(p(\mathbf{x}))$	$J(\mathbf{x}) = \frac{\nabla_{\mathbf{x}} p(\mathbf{x})}{p(\mathbf{x})}$ $\nabla_{\mathbf{x}} \log(p(\mathbf{x}))$	$p(\mathbf{x})^{-1}$ $-\log(p(\mathbf{x}))$	$\mu(\mathbf{x})$ $\log(\mu(\mathbf{x}))$	$\frac{1}{\mu(\mathbf{x})} \Sigma(\mathbf{x})$ $\frac{1}{\mu(\mathbf{x})} B \cdot \lambda \cdot B^{\top}$	$\frac{1}{\mu(\mathbf{x})} B \cdot \log(\lambda) \cdot B^{\top}$ $\int_{\mathbf{x}}^{\tilde{\mathbf{x}}} p(\mathbf{x}') d\mathbf{x}'$ $\int_{\mathbf{x}}^{\tilde{\mathbf{x}}} \log(p(\mathbf{x}')) d\mathbf{x}'$

The obvious factor that generates the vision process is the *energy*. In statistical terms, **(iv) the first moment (mean) of the signal**. The first eigenvalue of the manifold of a class of images represents the average luminance of the scene. The consideration of the nonlinear brightness-from-luminance is a fundamental law in visual psychophysics (the Weber-Fechner law [74, 17]), it has statistical explanations related to the cumulative density [36, 43, 31] and using empirical estimation of reflectance [55], and adaptivity of brightness curves [75] can only be described using sophisticated non-linear architectures [25, 49, 6].

Beyond the obvious *energy*, vision is about understanding the *spatial structure*. The simplest statistical description of the structure is, **(v) the second moment (or covariance) of the signal**. The (roughly) stationary invariance of natural images implies that the covariance can be diagonalized in Fourier like-basis, $\Sigma(\mathbf{x}) = B \cdot \lambda \cdot B^{\top}$ [13], and that the spectrum of eigenvalues in λ represents the average Fourier spectrum of natural images. The magnitude of the sinusoidal components compared to the mean luminance is the concept of *contrast* [50, 53], which is central in human spatial vision, which has a distinct bandwidth [11], which has been study of specific statistical explanations related to the spectrum of natural images [1, 20, 37].

Finally, classical generative models of natural images in the 90's and 00's used **(vi) heavy-tailed marginal PDFs in transformed domains** [62, 42, 26, 68] and then these marginal models were combined through mixing matrices (either PCA, DCT, ICA or wavelets), conceptually represented in the table by the matrix B . In this context, the response of a visual system (again according to PDF uniformization principles) should be related to non-linear saturations of the average spectrum (to compensate the high population at zero contrast) or cumulative functions of the marginals. These explanations [58, 43] have been given for the adaptive nonlinearities that happen in the wavelet-like representation in the visual cortex [22, 12], and also to define perceptual metrics [14, 64, 46, 35, 29].

2.3. Our proposal

What we propose in this work is using the kind of *descriptors* recalled in Table 1 (mainly PDFs of images, log-likelihoods, their directional derivatives, cumulative functions, and 1st and 2nd order moments, eventually subjected to saturating nonlinearities) as the subject of our study to predict the *sensitivity* of state-of-the-art perceptual distances, through information-theory and machine learning feature selection tools and using state-of-the-art generative models for PDF estimation.

Of course the exploration of all the variations of the specific formulations introduced in the literature review associated to Table 1 is out of the scope of a conference paper, and, as a proof of concept, in this work we will use the generative models to compute the following list of descriptors involving the original image \mathbf{x} and the distorted image $\tilde{\mathbf{x}}$:

$$\log(p(\mathbf{x})) , \log(p(\tilde{\mathbf{x}})) , \|J(\mathbf{x})\| , \|J(\tilde{\mathbf{x}})\| , \\ (\mathbf{x} - \tilde{\mathbf{x}})^{\top} \cdot J(\mathbf{x}) , \mu(\mathbf{x}) , \sigma(\mathbf{x}) , \int_{\mathbf{x}}^{\tilde{\mathbf{x}}} \log(p(\mathbf{x}')) d\mathbf{x}' \quad (2)$$

where $J(\mathbf{x})$ is the (vector) gradient of the loglikelihood at \mathbf{x} as shown in Table 1, and the first descriptor of the 2nd row is the projection of that gradient in the direction of the distortion. Moreover, the standard deviation of the image, $\sigma(\mathbf{x})$ as a single element of the covariance $\Sigma(\mathbf{x})$ in Table 1, together with $\mu(\mathbf{x})$ capture the concept of RMSE contrast [53] (a generalization of the Michelson contrast [50]), and the integral takes the loglikelihood that can be computed from the generative models and accumulates it along the direction of distortion, qualitatively following the idea of cumulative responses proposed in equalisation methods [36, 43, 31, 34].

2.4. Illustrative perceptual distances

The most successful perceptual distances can be classified in four big families: **(i) Physiological-psychophysical architectures**. These include [14, 73, 64, 46, 35, 48,

[23] and in particular it includes NLPD [29], which consists of a sensible filterbank of biologically meaningful receptive fields and the canonical Divisive Normalization used in neuroscience [12]. **(ii) Descriptions of the statistical structure of the images.** These include, the popular SSIM [71], its (improved) multiscale version MS-SSIM [72], and recent version using deep learning: DISTs [15]. **(iii) Information-theoretic measures.** These include measures of transmitted information such as VIF [61, 44], and recent measures based on enforcing informational continuity in frames of natural sequences, such as PIM [7]. **(iv) Regression models:** generic deep architectures used for vision tasks retrained to reproduce human opinion on distortion as LPIPS [77].

In this work we use recent representative examples of the four families: Table 2 illustrates their performance in reproducing human perception. Fig. 1 shows an example of how the visual sensitivity to noise highly depends on the image and is well captured by a representative D_p measure, NLPD [29], but not by the Euclidean distance, RMSE.

2.5. Illustrative generative model

Most recent generative models aim at capturing the PDF around certain images, for example, human faces or bedrooms [27]. However, not only do these sets not cover natural images, they consist of a rigid structure when describing images as a whole. Rather, we follow the methodology in [24] and rely on a probability model which we know is accurate for the images we wish to query. PixelCNN++ [57] is trained on CIFAR10 [28], a dataset made up of colour images of size $(32 \times 32 \times 3)$ covering 10 classes of a wide range of natural images. This model has been shown to compress CIFAR10 samples to a low entropy, meaning the model has a good understanding of this kind of images. In order to trust the probabilities employed throughout this paper, we use images of the same kind as in CIFAR10 to ensure our log-likelihoods are accurate. Fig. 1 shows that cluttered images are successfully identified as less probable than smooth images by PixelCNN++, consistently with the known average spectrum of natural images [13, 1, 42, 63].

2.6. Distorted images

There are two factors to balance when looking at distortions around image \mathbf{x} so that the definition of *perceptual sensitivity* is meaningful. First; in order to understand the

Table 2. Performance of the considered D_p 's. We show Pearson and Spearman correlations with human opinion in TID2013 [54], and agreement with human judgement (in %) in BAPPS [77].

	MSSSIM	NLPD	PIM	LPIPS	DISTS
TID2013 ρ_p (ρ_s)	0.78 (0.80)	0.84 (0.80)	0.62 (0.65)	0.74 (0.67)	0.86 (0.83)
BAPPS (%)	61.7	61.5	64.5	69.2	69.0

ratio in Eq. 1 as a variation *per unit of euclidean distortion* proposed in [24], we need the distorted image $\tilde{\mathbf{x}}$ to be close to the original \mathbf{x} . Secondly, the perceptual distances are optimised to recreate human judgements, so if the distortion is too small and humans are not able to see it (or too big so that the image is totally destroyed), the distances are not trustworthy.

As such, we propose to use additive uniform noise on the surface of a sphere around \mathbf{x} of radius ϵ . We choose ϵ in order to generate $\tilde{\mathbf{x}}$ where the noise is small for humans ($\epsilon = 0.2$). Examples of the images and the noisy images can be seen in Fig. 1. Note that in order to use the perceptual distances and PixelCNN++, the images must fall within a range. After adding noise we apply clipping so the range of images is $[-1, 1]$, and only keep the images whose Euclidean distance is comparable. If an image has a large number of pixels that require clipping after noise, the Euclidean distance between \mathbf{x} and $\tilde{\mathbf{x}}$ will be noticeably different to the other images in the dataset. As such we only use images where $\text{RMSE} > 0.017$, resulting in 48,046 images.

3. Experiments

Firstly, we empirically show the behaviour of the perceptual sensitivity and probability using conditional histograms and use measures from information theory to show which probability surrogates are most related to perceptual sensitivity. Then we explore unconstrained polynomial combinations of these surrogates using machine learning regression models. Lastly, constrain ourselves to only consider the most important probability surrogates and identify sim-

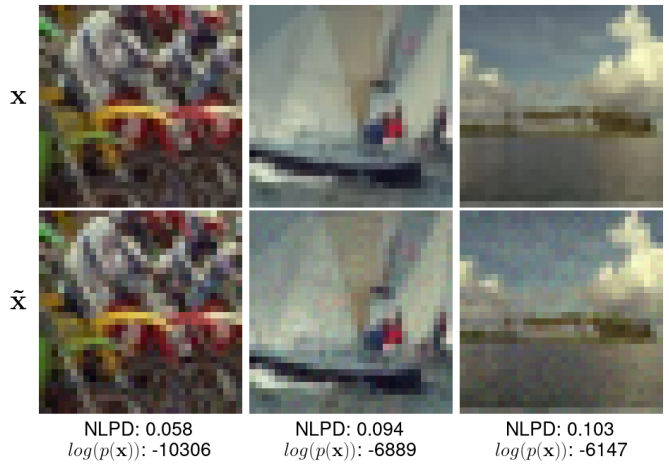


Figure 1. **The concept: visual sensitivity maybe bigger in more probable images.** Images where $\log(p(\mathbf{x}))$ is computed with PixelCNN++ [57], corrupted by uniform noise on the surface of sphere around \mathbf{x} of radius $\epsilon = 0.2$, with the same RMSE=0.018 (in $[0, 1]$ range). Due to the *masking phenomenon* [48], noise of the same energy is more visible, i.e. human sensitivity is bigger for smooth images (consistent with the NLPD distance [29], which are also more probable images (see the $\log(p(\mathbf{x}))$)).

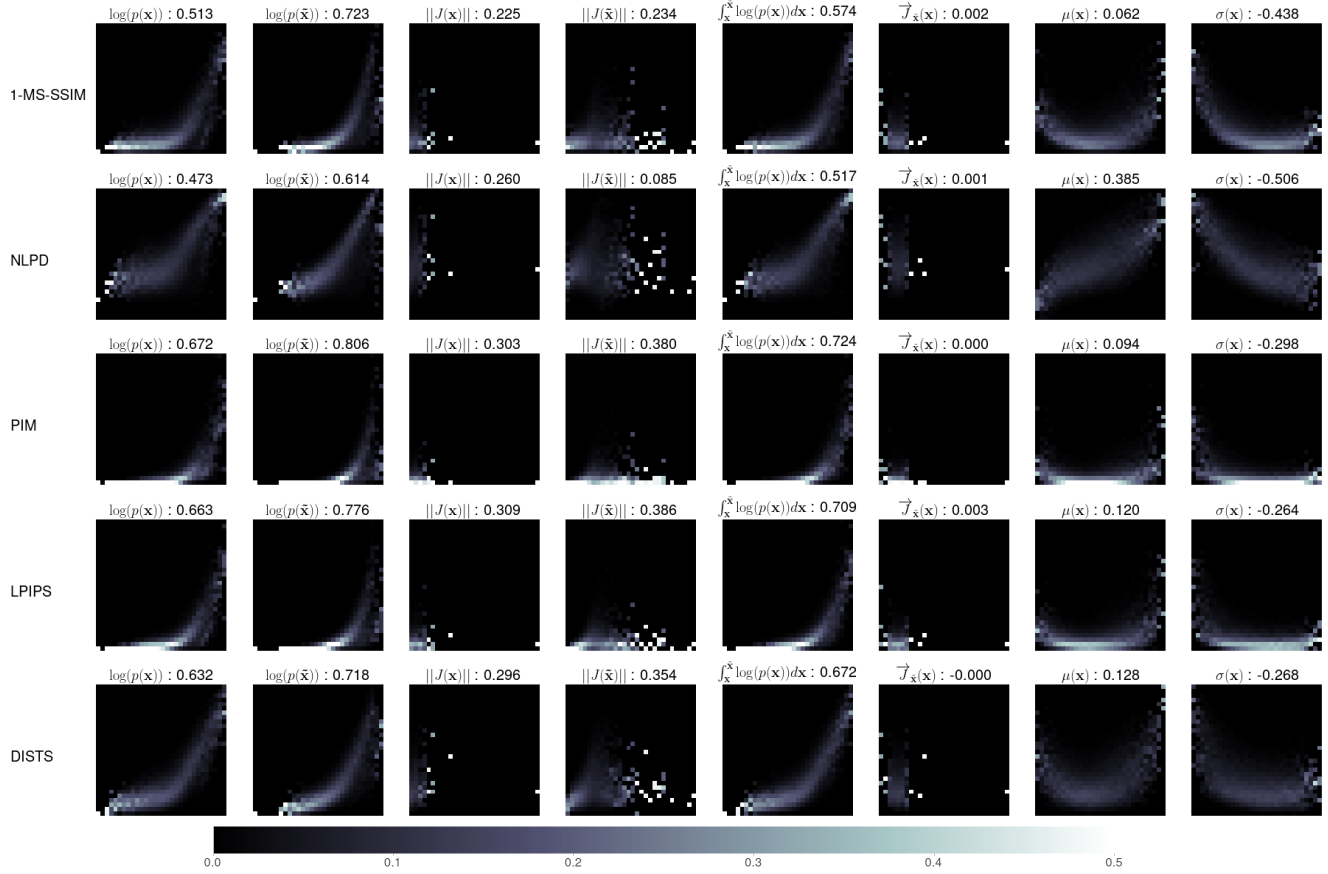


Figure 2. Conditional histograms where the x-axis is the probability surrogate (or image descriptor), and y-axis is perceptual sensitivity (Eq. 1) with just visible noise ($\epsilon = 0.2$). Also shown is the Spearman correlation between probability surrogate and perceptual sensitivity.

ple functional forms to predict perceptual sensitivity.

3.1. Conditional Histogram

Conditional histograms (Fig. 2.6) allow us to inspect the conditional distribution. In this case, we calculate $\mathcal{P}[S \in [b_{j-1}, b_j] | X = x]$ where S is the perceptual sensitivity partitioned into $m = 30$ bins $[b_{j-1}, b_j]$, X is one of the possible probability surrogates. This allows us to visually inspect which of the probability surrogates or image descriptors are important for predicting sensitivity. The probability surrogate used is given in each subplot title alongside the Spearman correlation between perceptual sensitivity and the surrogate.

For all perceptual distances, $\log(p(\mathbf{x}))$ has a high correlation, and mostly follows a similar conditional distribution. NLPD is the only distance that significantly differs, with more sensitivity in mid-probability images. We also see a consistent increase in correlation and conditional means when looking at $\log(p(\tilde{\mathbf{x}}))$, meaning the log-likelihood of the noisy sample is more indicative of perceptual sensitivity for all tested distances. Also note that the standard deviation $\sigma(\mathbf{x})$ also has a strong (negative) correlation across the

traditional distances, falling slightly with the deep learning based approaches. This is likely due to the standard deviation being closely related to the contrast of an image [50]. Note that measures that take into account both points, $\int_{\mathbf{x}}^{\tilde{\mathbf{x}}} \log(p(\mathbf{x})) d\mathbf{x}$ and $\overrightarrow{J}_{\tilde{\mathbf{x}}}(\mathbf{x})$, have lower correlation than just taking into account the noisy sample, with the latter being insignificant in predicting perceptual sensitivity.

3.2. Mutual Information Analysis

To quantify the probability surrogates ability to predict perceptual sensitivity, we use information theoretic measures. Firstly, we use mutual information which avoids the definition of a particular functional model and functional forms of the features. This analysis will give us insights into which of the factors derived from the statistics of the data can be useful in order to later define a functional model that relates statistics and perception.

Here, we analyse the mutual information between the different probability surrogates and the sensitivity of the distances. The idea is to find which surrogates will allow us to better predict perceptual sensitivity. The mutual information has been computed using all 48,046 samples and using

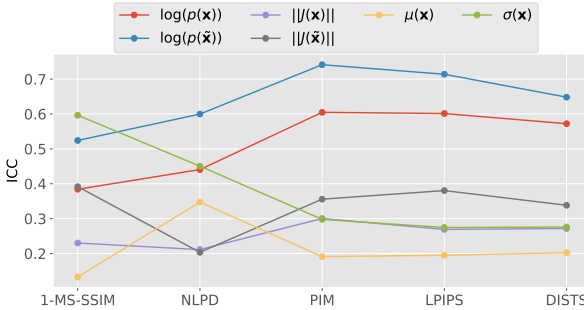


Figure 3. Information coefficient of correlation (ICC) between proposed probability surrogates and the sensitivity of different perceptual distances.

the Gaussianisation technique rotation based iterative Gaussianisation (RBIG) [30] as detailed here [33]. Instead of the mutual information value, we report the Information coefficient of correlation [38] (ICC) since the interpretation is similar to the Pearson coefficient and allows for easy comparison.

Figure 3 shows the ICC between each isolated probability surrogate and the sensitivity of different IQMs. It is clear that the most important factor to take into account in most models (second in MS-SSIM) is the probability of the noisy image $\log(p(\tilde{x}))$, a consistent result with the conditional histograms. Once we select the $\log(p(\tilde{x}))$ as the most important factor, we have to explore which other surrogate should be included as the second term. In order to do so we analyse the mutual information between each possible pair combination of surrogates with each IQM, results are shown in Fig. 4. It is clear that on the one hand the pairs where $\log(p(\tilde{x}))$ is involved have the maximum mutual information as concluded before, and the maximum is achieved when combining with the standard deviation of the original image $\sigma(x)$. This is true for four out of five models, again MS-SSIM is the one that differs.

Now we consider the third and the fourth factors to include. Fig 5 shows the ICC when taking into account 3 factors. It is clear that the factor that adds more to the ICC is $\log(p(x))$. In the case of the fourth factor (Fig. 6), the one that is more relevant is $\mu(x)$. Therefore we have this ordering of factors to take into account; $\{\log(p(\tilde{x})), \sigma(x), \log(p(x)), \mu(x)\}$. Table 3 shows the summary of the values of the ICC. In particular, we see that using only the $\log(p(\tilde{x}))$ we can capture between $[0.55 - 0.71]$ of the information. The difference between using one factor or more is not big.

In the following sections, we analyse the relations using machine learning regression models and study possible functional forms that include one or two factors and their effect on the predictability of the perceptual sensitivity.

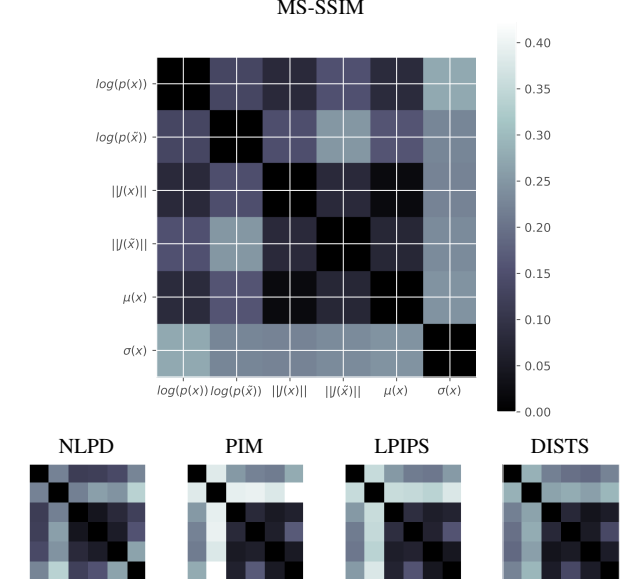


Figure 4. ICC between pairs of probability surrogates and the sensitivity of different metrics. The top figure shows the correspondence between rows and columns, and surrogates. The color bar is the same for all figures.

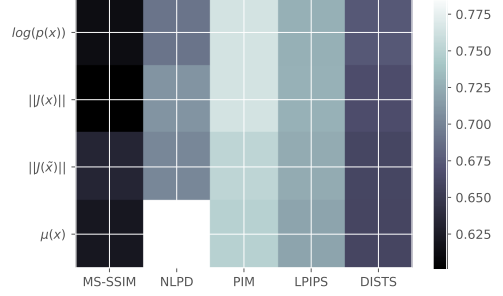


Figure 5. ICC 3 factors. Analysis of the shared information between sensitivity and 3 probability surrogates; $\{\log(p(x)), \sigma(x), f_s\}$ where f_s is one of the 4 possible probability surrogates in the y-axis.

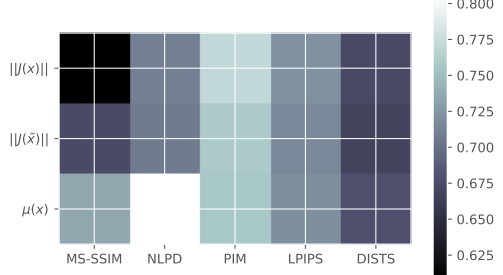


Figure 6. ICC 4 factors. Analysis of the shared information between sensitivity and 4 probability surrogates; $\{\log(p(x)), \sigma(x), \log(p(\tilde{x})), f_s\}$ where f_s is one of the 3 possible probability surrogates in the y-axis.

Table 3. Information coefficient of correlation [38] (ICC) between the sensitivity and the probability surrogates. Each row includes the factor that maximises the ICC, 1D: $\log(p(\tilde{x}))$, 2D: $\{\log(p(\tilde{x}), \sigma(x)\}$, 3D: $\{\log(p(\tilde{x}), \sigma(x), \log(p(\mathbf{x}))\}$, 4D: $\{\log(p(\tilde{x}), \sigma(x), \log(p(\mathbf{x})), \mu(x)\}$, 5D: $\{\log(p(\tilde{x})), \sigma(x), \log(p(\mathbf{x})), \mu(x), ||J(x)||\}$, and 6D all of them.

Factors	MS-SSIM	NLPD	PIM	LPIPS	DISTS	mean
1D	0.55	0.57	0.71	0.68	0.61	0.62
2D	0.57	0.66	0.72	0.69	0.63	0.65
3D	0.68	0.68	0.72	0.69	0.65	0.68
4D	0.68	0.76	0.75	0.71	0.66	0.71
5D	0.68	0.78	0.75	0.73	0.66	0.72
6D	0.71	0.79	0.76	0.73	0.66	0.73

3.3. Regression

We explore simple interpretable models and how probability surrogates can be combined in order to predict perceptual sensitivity. In order to do so, we fit a random forest regressor [8], with the probability surrogates and polynomial combinations with order 2, and optimise the regressor to predict the perceptual sensitivity. The inverse probability for both original and noisy images is also included. Regression trees are convenient for this task since it is easy to analyse the relevance of each feature and compare between models trained on different perceptual sensitivities. Feature importances are normalised so that they sum to 1 for each model for easy comparison. We use a held out test set of 30% dataset in order to calculate correlations between predicted and ground truth. Figure 7 shows the 6 probability surrogates with the most importance across perceptual distances and their relevant importance for each IQM, and the Pearson (Spearman) correlation that indicates how good the model is at predicting perceptual sensitivity. The average Pearson correlation is 0.85, this can be compared with models proposed in Section 4. It can be seen that $\log(p(\tilde{x}))$ is by far the most important which agrees with what was found in the mutual information analysis (sec. 3.2). It has been suggested that the derivative of the log-likelihood should be important, given those modifications in the slope of the distribution imply label change and the score-matching objective makes use of the gradient [69]. However, we find that the derivative has low shared mutual information and low feature influence.

4. Functional relation

Given the mutual information results (Sec. 3.2) and the machine learning regression exploration (Sec. 3.3), here we explore the actual functional form that can extract that information. As a reference, the Random Forest regressor fit with all the factors and polynomial combinations up to factor 2 (Sec. 3.3) obtains an average correlation among the IQMs of 0.84, which can be taken as an upper bound. We conduct an ablation study, training a linear regressor on the most important factors and ablating each factor in order to

Table 4. Pearson correlation obtained between the prediction of the model and the sensitivity for different IQMs. All models are designed using versions of $\log(p(\tilde{x}))$ as input factor, the models are polynomials of different degrees (d) or polynomials with specific exponents. The degrees of the polynomial or the exponents (γ) employed are given in the first column. The model *Frac** uses as exponents (γ): [0.3, 0.2, 0.1, 0.1, 2, 3].

	MSSIM	NLPD	PIM	LPIPS	DISTS	mean
d = 1	0.7	0.63	0.65	0.68	0.72	0.68
d = 2	0.76	0.65	0.75	0.76	0.74	0.73
d = 3	0.76	0.65	0.75	0.75	0.74	0.73
d = 6	0.75	0.64	0.73	0.74	0.74	0.72
<i>Frac*</i>	0.76	0.65	0.76	0.76	0.74	0.73
$\gamma = 1/10$	0.71	0.64	0.66	0.69	0.72	0.68
$\gamma = 1/5$	0.71	0.64	0.66	0.69	0.72	0.68
$\gamma = 1/3$	0.71	0.64	0.66	0.69	0.72	0.68
$\gamma = 1/2$	0.71	0.63	0.66	0.69	0.72	0.68
$\gamma = 2$	0.69	0.63	0.64	0.68	0.71	0.67
$\gamma = -1$	0.72	0.65	0.66	0.71	0.73	0.69

create various closed form expressions of perceptual sensitivity. We keep factors that maximise the Pearson correlation between the model’s predictions and the ground truth.

4.1. One-factor model

The factor with the highest ICC and feature importance is $\log(p(\tilde{x}))$. We explore different polynomials to predict sensitivity where the different factors are forms of $p(\tilde{x})$. Results are shown in Table 4. The correlation goes from around 0.68 for models with only one degree (i.e. $S(\mathbf{x}, \tilde{\mathbf{x}}) = w_0 + w_1 \log(p(\tilde{\mathbf{x}}))^\gamma$ where $\gamma = \{1, \frac{1}{10}, \frac{1}{5}, \frac{1}{3}, \frac{1}{2}, 2, -1\}$), to 0.73 which can be obtained with a simple polynomial of degree two ($d = 2$). Therefore the selected candidate would be:

$$S(\mathbf{x}, \tilde{\mathbf{x}}) = w_0 + w_1 \log(p(\tilde{\mathbf{x}})) + w_2 \log(p(\tilde{\mathbf{x}}))^2, \quad (3)$$

with an average correlation of 0.73. The exact weights for each perceptual distance can be seen in the Appendix.

4.2. Two-factors model

The two factors that contain the most information about the sensitivity are $\log(p(\tilde{x}))$ and $\sigma(\mathbf{x})$. We explore multiple possible functional forms that include combinations of both factors. Note that the possible functional form candidates are intractable. Here we restrict ourselves to polynomials that include the simpler versions of these factors isolated, i.e. $\{\log(p(\tilde{x})), \log(p(\tilde{x}))^2\}$ and $\{\sigma(\mathbf{x}), \sigma(\mathbf{x})^2, \sigma(\mathbf{x})^{-1}\}$, and the simplest products and divisions using both.

The analysis of multiple models that include these combinations as well as a LASSO [65] exploration can be seen in the Appendix. In conclusion, a model that combines good predictions and simplicity is the one that adds the $\sigma(\mathbf{x})$ factor to the model suggested in the previous Section 4.1. This model obtains a 0.79 mean correlation:

$$S(\mathbf{x}, \tilde{\mathbf{x}}) = w_0 + w_1 \log(p(\tilde{\mathbf{x}})) + w_2 \log(p(\tilde{\mathbf{x}}))^2 + w_3 \sigma(\mathbf{x}) \quad (4)$$

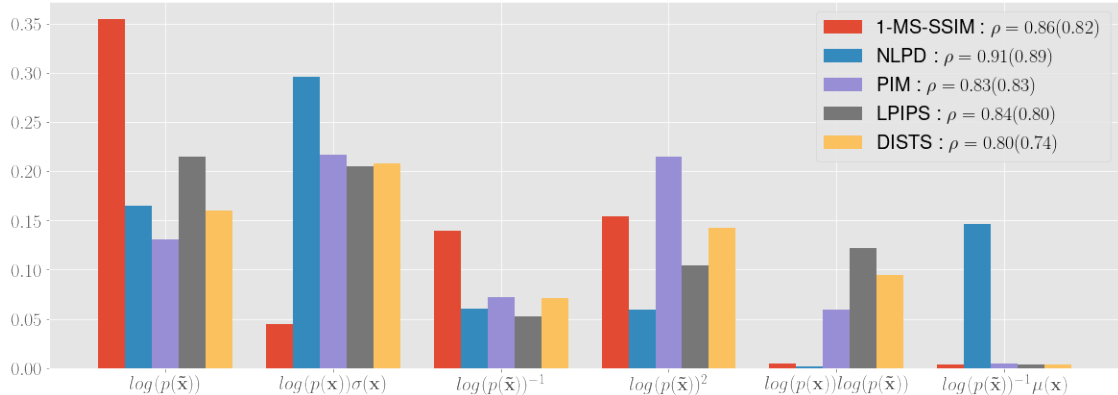


Figure 7. Top 6 feature importances from a Random Forest regressor trained on polynomial combinations of the probability surrogates in order to predict perceptual sensitivity. A separate model was trained for each perceptual distance. In the legend we include the Pearson (Spearman) correlation between the predictions and ground truth for a held out test set 30% of the dataset.

This implies an increase of 0.06 in correlation in regard to the model that only includes $\log(p(\tilde{x}))$. As a reference, a model that includes all nine analysed combinations for the two factors obtains a 0.81 correlation.

5. Conclusion

We show that the probability surrogates and the perceptual sensitivity of various IQMs share substantial information, with a mean ICC of 0.73. Alongside this, a Random Forest regressor that predicts sensitivity using only polynomial combinations of simple probability surrogates can obtain an average Pearson correlation between the predicted sensitivity and the ground truth of 0.85 (Sec. 3.3). These numbers are surprisingly high given that it is clear that not only the statistics of the input data are going to determine the perceptual behaviour. For instance, different animals in the same environment have different visual perception [16]. In contrast to existing literature [69], we find that the derivative has low shared mutual information and low feature influence. The most relevant factor found is the probability of the noisy image, $\log(p(\tilde{x}))$. Intuitively this makes sense, since this measure simultaneously includes information on the distribution of the original image (since we are in a differential context so the two log-likelihoods should be similar), and information about the specific direction the included noise has affected the distribution. This isolated factor obtains an average ICC of 0.62, and a simple model including this factor to predict sensitivity achieves a 0.73 Pearson correlation with the ground truth. This model is a simple polynomial of degree 2. Given the mutual information analysis, the factors can be ordered by relevance as: $\{\log(p(\tilde{x})), \sigma(x), \log(p(x)), \mu(x), \|J(x)\|\}$. This is in agreement with the relevance given by a regression tree model that uses the same features, including polynomial combinations of them.

After an ablation study using the factors with the highest ICC values, we propose a simple functional form (Eq. 3) using only the probability of the noisy image $\log(p(\tilde{x}))$ that obtains 0.73. Adding the second most relevant factor, the standard deviation of the original image $\sigma(x)$, increases the correlation up to 0.79 (Eq. 4).

This study is limited on the one hand by the probability model used (PixelCNN++), which was trained using small images, a restricted set of images (CIFAR10), with a restricted luminance range. In order to have more trustable results in terms of image probability we limited ourselves to using the same type of images that the model was trained for. On the other hand, as a proxy for human perception we have to use IQMs. Although their correlation with MOS is not bad (see Table 2), these models are far from perfect. The ideal situation would be experimenting with humans, a simple way could be using image quality databases (such as TID2013 or KADID10k) but the images are too big for probability models currently. Besides in these databases, the number of images is smaller and the experiments are not done in a well controlled setup (for instance it is not clear what the luminance for each image pixel in the experimental screen is).

Beyond the previously established connection between probability and perception, in this work, we provide methods to quantify this relationship. We analyse the mutual information between various IQMs and probability surrogates, and look at the performance of probability surrogates in predicting perceptual sensitivity. We identify a number of factors that are strongly linked and perform an ablation study in order to propose function forms for perceptual sensitivity that depend only on probability, with a strong correlation between the ground truth and predicted sensitivity. These models shed light on the link between statistics and perception.

References

[1] JJ. Atick, Z. Li, and AN. Redlich. Understanding retinal color coding from first principles. *Neural Comp.*, 4(4):559–572, 1992. 1, 2, 3, 4

[2] J J Atick. Could information theory provide an ecological theory of sensory processing? *Network: Computation in Neural Systems*, 3(2):213, 1992. 2

[3] F. Attnave. Some informational aspects of visual perception. *Psychological Review*, 61(3), 1954. 1

[4] H. B. Barlow. Possible principles underlying the transformation of sensory messages. *Sensory Communication*, pages 217–234, 1961. 1, 3

[5] Anthony J. Bell and Terrence J. Sejnowski. The ‘independent components’ of natural scenes are edge filters. *Vision Research*, 37(23):3327–38, 1997. 1, 2, 3

[6] M. Bertalmío, A. Gomez-Villa, and J. et al. Malo. Evidence for the intrinsically nonlinear nature of receptive fields in vision. *Scientific Reports*, 10:16277, 2020. 3

[7] S. Bhardwaj, I. Fischer, J. Ballé, and T. Chinen. An unsupervised information-theoretic perceptual quality metric. In *Adv. Neur. Inf. Proc. Syst. (NeurIPS)*, volume 33, pages 13–24, 2020. 4

[8] Leo Breiman. Random forests. *Machine learning*, 45:5–32, 2001. 7

[9] Neil Bruce and John Tsotsos. Saliency based on information maximization. In *Advances in Neural Information Processing Systems*, volume 18. MIT Press, 2005. 1, 2, 3

[10] G. Buchsbaum and A. Gottschalk. Trichromacy, opponent colours coding and optimum colour information transmission in the retina. *Proc. Roy. Soc. Lond. B Biol. Sci.*, 220(1218):89–113, 1983. 1, 2

[11] F. W. Campbell and J. G. Robson. Application of Fourier analysis to the visibility of gratings. *The Journal of Physiology*, 197(3):551–566, 1968. 3

[12] M. Carandini and D. Heeger. Normalization as a canonical neural computation. *Nature Reviews. Neurosci.*, 13(1):51–62, 2012. 3, 4

[13] R.J. Clarke. Relation between the karhunen loève and cosine transforms. *IEE Proc. F*, 128(6):359–360, 1981. 3, 4

[14] Scott J. Daly. Application of a noise-adaptive contrast sensitivity function to image data compression. *Optical Engineering*, 29(8):977 – 987, 1990. 3, 4

[15] K. Ding, K. Ma, S. Wang, and E. P. Simoncelli. Image quality assessment: Unifying structure and texture similarity. *arXiv preprint arXiv:2004.07728*, 2020. 1, 2, 4

[16] Jonathan T. Erichsen and J. Margaret Woodhouse. *Human and Animal Vision*, pages 89–115. Springer London, London, 2012. 8

[17] Gustav Theodor Fechner. *Elements of psychophysics. Volume 1 / Gustav Fechner ; translated by Helmut E. Adler ; edited by David H. Howes, Edwin G. Boring ; with an introduction by Edwin G. Boring*. Holt, Rinehart and Winston, Inc., New York, 1860. 3

[18] Deep Ganguli and Eero P. Simoncelli. Efficient sensory encoding and bayesian inference with heterogeneous neural populations. *Neural Comput.*, 26(10):2103–2134, 2014. 2

[19] Karl R Gegenfurtner and Jochem Rieger. Sensory and cognitive contributions of color to the recognition of natural scenes. *Current Biology*, 10(13):805–808, 2000. 2, 3

[20] A. Gomez-Villa, A. Martín, J. Vazquez-Corral, M. Bertalmío, and J. Malo. Color illusions also deceive CNNs for low-level vision tasks: Analysis and implications. *Vision Research*, 176:156 – 174, 2020. 3

[21] P J B Hancock, R J Baddeley, and L S Smith. The principal components of natural images. *Network: Computation in Neural Systems*, 3(1):61, 1992. 2

[22] David Heeger. Normalization of cell responses in cat striate cortex. *Vis. Neurosci.*, 9(2):181–197, 1992. 3

[23] Alexander Hepburn, Valero Laparra, Jesús Malo, Ryan McConvile, and Raúl Santos-Rodríguez. Perceptnet: A human visual system inspired neural network for estimating perceptual distance. In *IEEE ICIP 2020*, pages 121–125. IEEE, 2020. 1, 2, 4

[24] Alexander Hepburn, Valero Laparra, Raul Santos-Rodriguez, Johannes Ballé, and Jesus Malo. On the relation between statistical learning and perceptual distances. In *International Conference on Learning Representations*, 2022. 1, 2, 3, 4

[25] James M. Hillis and David H. Brainard. Do common mechanisms of adaptation mediate color discrimination and appearance? uniform backgrounds. *J. Opt. Soc. Am. A*, 22(10):2090–2106, 2005. 3

[26] Aapo Hyvärinen, Jarmo Hurri, and Patrick O Hoyer. *Natural image statistics: A probabilistic approach to early computational vision.*, volume 39. Springer Science & Business Media, 2009. 1, 2, 3

[27] Durk P Kingma and Prafulla Dhariwal. Glow: Generative flow with invertible 1x1 convolutions. *Advances in neural information processing systems*, 31, 2018. 4

[28] A. Krizhevsky, G. Hinton, et al. Learning multiple layers of features from tiny images. 2009. 4

[29] V. Laparra, J. Ballé, A. Berardino, and Simoncelli E P. Perceptual image quality assessment using a normalized laplacian pyramid. *Electronic Imaging*, 2016(16):1–6, 2016. 1, 3, 4

[30] Valero Laparra, Gustavo Camps-Valls, and Jesús Malo. Iterative gaussianization: from ica to random rotations. *IEEE transactions on neural networks*, 22(4):537–549, 2011. 6

[31] V. Laparra, S. Jiménez, G. Camps, and J. Malo. Nonlinearities and adaptation of color vision from sequential principal curves analysis. *Neural Comp.*, 24(10):2751–2788, 2012. 2, 3

[32] Valero Laparra, Sandra Jiménez, Gustavo Camps-Valls, and Jesús Malo. Nonlinearities and adaptation of color vision from sequential principal curves analysis. *Neural Computation*, 24(10):2751–2788, 2012. 3

[33] Valero Laparra, J Emmanuel Johnson, Gustau Camps-Valls, Raul Santos-Rodríguez, and Jesus Malo. Information theory measures via multidimensional gaussianization. *arXiv preprint arXiv:2010.03807*, 2020. 6

[34] V. Laparra and J. Malo. Visual aftereffects and sensory nonlinearities from a single statistical framework. *Frontiers in Human Neuroscience*, 9:557, 2015. 1, 2, 3

[35] V. Laparra, J. Muñoz-Marí, and J. Malo. Divisive normalization image quality metric revisited. *J. Opt. Soc. Am. A*, 27(4):852–864, 2010. 3, 4

[36] S. Laughlin. A simple coding procedure enhances a neuron's information capacity. *Zeit. Natur. C, Biosciences*, 36(9-10):910—912, 1981. [1](#), [2](#), [3](#)

[37] Qiang Li, Alex Gomez-Villa, Marcelo Bertalmío, and Jesús Malo. Contrast sensitivity functions in autoencoders. *Journal of Vision*, 22(6), 05 2022. [3](#)

[38] E.H. Linfoot. An informational measure of correlation. *Information and Control*, 1(1):85–89, 1957. [6](#), [7](#)

[39] S. Lloyd. Least squares quantization in pcm. *IEEE Transactions on Information Theory*, 28(2):129–137, 1982. [1](#), [2](#), [3](#)

[40] Donald Ia Macleod and Tassilo von der Twer. The pleistochrome: Optimal opponent codes for natural colours. In Mausfeld and Heyer, editors, *Colour Perception: Mind and the Physical World*. Oxford University Press, 2003. [2](#), [3](#)

[41] B. Macq. Weighted optimum bit allocations to orthogonal transforms for picture coding. *IEEE Journal on Selected Areas in Communications*, 10(5):875–883, 1992. [2](#)

[42] J. Malo, F. Ferri, J. Albert, J. Soret, and J.M. Artigas. The role of perceptual contrast non-linearities in image transform quantization. *Image and Vision Computing*, 18(3):233–246, 2000. [2](#), [3](#), [4](#)

[43] Jesús Malo and Juan Gutiérrez. V1 non-linear properties emerge from local-to-global non-linear ica. *Network: Computation in Neural Systems*, 17(1):85–102, 2006. [2](#), [3](#)

[44] J. Malo, B. Kheravdar, and Q. Li. Visual information fidelity with better vision models and better mutual information estimate. *J. Vision*, 21(9):2351, 2021. [4](#)

[45] J. Malo and V. Laparra. Psychophysically tuned divisive normalization approximately factorizes the pdf of natural images. *Neural computation*, 22(12):3179–3206, 2010. [2](#)

[46] J. Malo, A.M. Pons, and J.M. Artigas. Subjective image fidelity metric based on bit allocation of the human visual system in the dct domain. *Image and Vision Computing*, 15(7):535–548, 1997. [3](#), [4](#)

[47] David Marr and Tomaso Poggio. From understanding computation to understanding neural circuitry. *AI Memo No. AIM-357. MIT Libraries*, 1976. [1](#)

[48] M. Martinez, M. Bertalmío, and J. Malo. In praise of artifice reloaded: Caution with image databases in modeling vision. *Front. Neurosci.*, 13:1–17, 2019. [4](#)

[49] M. Martinez, P. Cyriac, T. Batard, M. Bertalmío, and J. Malo. Derivatives and inverse of cascaded linear+ nonlinear neural models. *PLoS ONE*, 13(10):e0201326, 2018. [3](#)

[50] AA. Michelson. *Studies in Optics*. U. Chicago Press, Chicago, Illinois, 1927. [3](#), [5](#)

[51] K. Miyasawa. An empirical bayes estimator of the mean of a normal population. *Bull. Inst. Internat. Statist.*, 38:181—188, 1961. [1](#), [2](#), [3](#)

[52] B.A. Olshausen and D.J. Field. Emergence of simple-cell receptive field properties by learning a sparse code for natural images. *Nature*, 381:607–609, June 1996. [1](#), [2](#)

[53] Eli Peli. Contrast in complex images. *J. Opt. Soc. Am. A*, 7(10):2032–2040, 1990. [3](#)

[54] N. Ponomarenko et al. Color image database tid2013: Peculiarities and preliminary results. In *EUVIP*, pages 106–111. IEEE, 2013. [4](#)

[55] Dale Purves, William T. Wojtach, and R. Beau Lotto. Understanding vision in wholly empirical terms. *Proceedings of the National Academy of Sciences*, 108(supplement_3):15588–15595, 2011. [3](#)

[56] Martin Raphan and Eero P. Simoncelli. Least Squares Estimation Without Priors or Supervision. *Neural Comp.*, 23(2):374–420, 02 2011. [2](#), [3](#)

[57] T. Salimans, A. Karpathy, X. Chen, and D. P. Kingma. PixelCNN++: Improving the pixelcnn with discretized logistic mixture likelihood and other modifications. *arXiv preprint arXiv:1701.05517*, 2017. [1](#), [4](#)

[58] O. Schwartz and E. Simoncelli. Natural signal statistics and sensory gain control. *Nature Neurosci.*, 4(8):819–825, 2001. [1](#), [3](#)

[59] Peggy Seriès, Alan A. Stocker, and Eero P. Simoncelli. Is the Homunculus “Aware” of Sensory Adaptation? *Neural Computation*, 21(12):3271–3304, 12 2009. [2](#)

[60] Claude Elwood Shannon. A mathematical theory of communication. *The Bell System Technical Journal*, 27:379–423, 1948. [2](#), [3](#)

[61] H. Sheikh and A. Bovik. Image information and visual quality. *IEEE Trans. Im. Proc.*, 15(2):430–444, Feb 2006. [4](#)

[62] E.P. Simoncelli. Statistical models for images: compression, restoration and synthesis. In *Conference Record of the Thirty-First Asilomar Conference on Signals, Systems and Computers (Cat. No.97CB36136)*, volume 1, pages 673–678 vol.1, 1997. [3](#)

[63] Eero P Simoncelli and Bruno A Olshausen. Natural image statistics and neural representation. *Annual review of neuroscience*, 24(1):1193–1216, 2001. [1](#), [4](#)

[64] P. Teo and D. Heeger. Perceptual image distortion. In *IEEE ICIP*, volume 2, pages 982–986, 1994. [3](#), [4](#)

[65] Robert Tibshirani. Regression shrinkage and selection via the lasso. *Journal of the Royal Statistical Society: Series B (Methodological)*, 58(1):267–288, 1996. [7](#)

[66] T. Twer and D. MacLeod. Optimal nonlinear codes for the perception of natural colours. *Network: Comp. Neur. Syst.*, 12(3):395–407, 2001. [1](#), [2](#), [3](#)

[67] Aäron van den Oord, Nal Kalchbrenner, and Koray Kavukcuoglu. Pixel recurrent neural networks. *CoRR*, abs/1601.06759, 2016. [1](#)

[68] Aäron van den Oord and Benjamin Schrauwen. The student-t mixture as a natural image patch prior with application to image compression. *Journal of Machine Learning Research*, 15(60):2061–2086, 2014. [3](#)

[69] Pascal Vincent. A Connection Between Score Matching and Denoising Autoencoders. *Neural Comp.*, 23(7):1661–1674, 07 2011. [2](#), [3](#), [7](#), [8](#)

[70] Zhou Wang and Alan C. Bovik. Mean squared error: Love it or leave it? a new look at signal fidelity measures. *IEEE Signal Processing Magazine*, 26(1):98–117, 2009. [2](#)

[71] Z. Wang, A. C. Bovik, H. R. Sheikh, and E. P. Simoncelli. Image quality assessment: from error visibility to structural similarity. *IEEE Trans. Image Process*, 13(4):600–612, April 2004. [2](#), [4](#)

[72] Z. Wang, E. P. Simoncelli, and A. C. Bovik. Multiscale structural similarity for image quality assessment. In *ACSSC*, volume 2, pages 1398–1402. Ieee, 2003. [2](#), [4](#)

- [73] A.B. Watson. *Digital images and human vision*. Cambridge, Mass. : MIT Press, 1993. 4
- [74] E. H. Weber. *The sense of touch and common feeling, 1846*, page 194–196. Appleton-Century-Crofts, NY, 1948. 3
- [75] Paul Whittle. Brightness, discriminability and the “crispening effect”. *Vision Research*, 32(8):1493–1507, 1992. 3
- [76] F.A. Wichmann, L.T. Sharpe, and K.R. Gegenfurtner. The contributions of color to recognition memory for natural scenes. *J. Experim. Psychol.: Learn., Memory, and Cognit.*, 28(3):509–520, 2002. 2, 3
- [77] R. Zhang, P. Isola, A. Efros, E. Shechtman, and O. Wang. The unreasonable effectiveness of deep features as a perceptual metric. In *Proceedings of the IEEE CVPR*, pages 586–595, 2018. 1, 2, 4

A. Functional forms coefficients.

In section 4 we propose Eq. 3 and Eq. 4 as estimators of the perceptual sensitivity for 1 and 2 factors respectively. Note that each IQM has a different interpretation of the sensitivity units, therefore the weights of the proposed equations are different for each measure. In tables 5 and 6 we give the actual weights obtained in the experiments for each IQMs. 1

B. Details on the selection of parameters for the functional form.

Here we show the details for the selection of the parameters in section 4. Note that first, we have to choose candidates for the polynomial fitting. We took the ones obtained in section 4.1 (i.e. b (bias), $\log(p(\tilde{x}))$, and $\log(p(\tilde{x}))^2$), and combinations the standard deviation σ_x as suggested by the mutual information in section 3.2. The combinations of the standard deviation have been alone: σ_x , $\frac{1}{\sigma_x}\sigma_x^2$, and combined with the probability of the noisy image: $\frac{\log(p(\tilde{x}))}{\sigma_x}$, $\frac{\sigma_x}{\log(p(\tilde{x}))}$, and $\log(p(\tilde{x}))\sigma_x$.

There are 9 candidates but we want the most compact and interpretable model. Analysing all the possible combinations is intractable so we are going to follow two strategies. On the one hand, we are going to discard different candidates sequentially starting from the largest model (9 candidates). On the other hand, we are going to use LASSO regression with different amounts of regularisation. Results in table 7 are shown in descending order in the number of factors taken into account. For each step, we remove the factor (or factors) that less influence has in the correlation. Besides, we show the correlation given by a LASSO model where the regularization parameter has been adjusted in order to have the same number of factors. A model with 6 factors (number 17) has the same correlation (0.81) than the one with all the factors (number 1). The best trade-off between the number of factors and correlation is with for the models 25, 26 and 27, with 4 factors and a correlation of

0.79. We chose as our final functional model in section 4.2 the model 25 as its factors involve less computations.

Table 5. Coefficients for the Eq. 3 for each IQM.

Coefs	MSSIM	NLPD	PIM	LPIPS	DISTS
b	29.5	65	15400	198	161
$\log(p(\tilde{x}))$	$4.9 \cdot 10^{-3}$	$9.5 \cdot 10^{-3}$	2.62	$3.33 \cdot 10^{-2}$	$2.58 \cdot 10^{-2}$
$\log(p(\tilde{x}))^2$	$2.05 \cdot 10^{-7}$	$3.62 \cdot 10^{-7}$	$1.11 \cdot 10^{-4}$	$1.41 \cdot 10^{-6}$	$1.05 \cdot 10^{-6}$

Table 6. Coefficients for the Eq. 4 for each IQM.

Coefs	MSSIM	NLPD	PIM	LPIPS	DISTS
b	28	58	15100	194	156
$\log(p(\tilde{x}))$	$4.69 \cdot 10^{-3}$	$8.19 \cdot 10^{-3}$	2.57	$3.26 \cdot 10^{-2}$	$2.49 \cdot 10^{-2}$
$\log(p(\tilde{x}))^2$	$1.96 \cdot 10^{-7}$	$3.09 \cdot 10^{-7}$	$1.09 \cdot 10^{-4}$	$1.37 \cdot 10^{-6}$	$1.00 \cdot 10^{-6}$
$\sigma(x)$	-0.597	-3.74	-141	-1.93	-2.54

Table 7. Linear models using different combinations of b (bias), $\log(p(\tilde{x})) = p$ and $\sigma(x) = s$, where 1 indicates the factor is included in the model, and 0 is ablated. Models with * in the model number (# Model) have been computed using lasso and a corresponding regularization parameter in order to have a particular number of combinations (# comb) of the parameters. Models are ordered by number of combinations in the model. For the perceptual metrics, reported is the Pearson correlation between the predicted and ground truth on a test set of CIFAR10.

b	p	p^2	s	s^2	$\frac{1}{s}$	$\frac{p}{s}$	$\frac{s}{p}$	ps	MSSIM	NLPD	PIM	LPIPS	DISTS	MEAN	# comb	#Model
1	1	1	1	1	1	1	1	1	0.85	0.78	0.81	0.81	0.78	0.806	9	1
1	1	1	0	1	1	1	1	1	0.85	0.78	0.81	0.81	0.78	0.806	8	2
1	1	1	1	0	1	1	1	1	0.85	0.78	0.81	0.81	0.78	0.806	8	3
1	1	1	1	1	0	1	1	1	0.85	0.78	0.81	0.81	0.78	0.806	8	4
1	1	1	1	1	1	0	1	1	0.85	0.78	0.81	0.81	0.78	0.806	8	5
1	1	1	1	1	1	1	0	1	0.85	0.78	0.8	0.8	0.78	0.802	8	6
1	1	1	1	1	1	1	1	0	0.85	0.78	0.8	0.8	0.78	0.802	8	7
0	1	1	1	1	1	1	1	0	0.83	0.75	0.77	0.77	0.77	0.778	7	8
1	0	1	1	1	1	1	1	0	0.82	0.78	0.77	0.78	0.77	0.784	7	9
1	1	0	1	1	1	1	1	0	0.82	0.78	0.76	0.77	0.76	0.778	7	10
1	1	1	0	1	1	1	1	0	0.84	0.78	0.8	0.8	0.78	0.8	7	11
1	1	1	1	0	1	1	1	0	0.85	0.78	0.8	0.8	0.78	0.802	7	12
1	1	1	1	1	0	1	1	0	0.85	0.78	0.8	0.8	0.78	0.802	7	13
1	1	1	1	1	1	0	1	0	0.85	0.78	0.8	0.8	0.78	0.802	7	14
1	1	1	1	1	1	1	0	0	0.84	0.78	0.8	0.8	0.78	0.8	7	15
0	1	1	1	1	1	1	1	0	0.84	0.79	0.78	0.8	0.78	0.798	7	16*
1	1	1	1	0	0	0	1	1	0.85	0.78	0.81	0.81	0.78	0.806	6	17
0	1	1	0	1	1	1	0	1	0.84	0.79	0.78	0.8	0.78	0.798	6	18*
1	0	1	1	0	0	0	0	1	0.84	0.78	0.78	0.79	0.77	0.792	5	19
1	1	0	1	0	0	0	1	1	0.84	0.78	0.78	0.79	0.77	0.792	5	20
1	1	1	0	0	0	0	1	1	0.84	0.78	0.8	0.8	0.78	0.8	5	21
1	1	1	1	0	0	0	0	1	0.84	0.78	0.8	0.8	0.78	0.8	5	22
1	1	1	1	1	0	0	0	1	0.84	0.78	0.8	0.8	0.78	0.8	5	23
0	1	1	0	0	1	1	0	1	0.83	0.79	0.78	0.8	0.78	0.796	5	24*
1	1	1	1	0	0	0	0	0	0.83	0.78	0.77	0.78	0.77	0.786	4	25
1	1	1	0	0	0	0	0	1	0.83	0.78	0.78	0.78	0.77	0.788	4	26
1	1	1	0	0	0	0	0	1	0.83	0.78	0.77	0.78	0.77	0.786	4	27
1	1	0	0	0	0	0	0	1	0.8	0.78	0.72	0.74	0.76	0.76	4	28
1	0	1	0	0	0	0	0	1	0.79	0.77	0.7	0.73	0.75	0.748	4	29
0	1	1	1	0	0	0	0	1	0.76	0.65	0.75	0.76	0.74	0.732	4	30
1	0	1	1	0	0	0	0	1	0.79	0.77	0.7	0.72	0.75	0.746	4	31
1	1	0	1	0	0	0	0	1	0.8	0.77	0.71	0.74	0.75	0.754	4	32
0	1	1	0	0	0	1	0	1	0.83	0.79	0.78	0.76	0.77	0.786	4	33*
1	1	1	0	0	0	0	0	0	0.76	0.65	0.75	0.76	0.74	0.732	3	34
1	1	0	0	0	0	0	1	0	0.79	0.77	0.69	0.72	0.75	0.744	3	35
1	1	0	0	0	0	0	0	1	0.78	0.77	0.68	0.71	0.75	0.738	3	36
1	1	0	1	0	0	0	0	0	0.79	0.77	0.69	0.71	0.75	0.742	3	37
1	0	1	0	0	0	0	0	1	0.78	0.77	0.68	0.7	0.74	0.734	3	38
1	0	1	0	0	0	0	0	1	0.78	0.77	0.68	0.71	0.74	0.736	3	39
1	0	1	1	0	0	0	0	0	0.78	0.77	0.68	0.71	0.74	0.736	3	40
1	0	0	0	0	0	0	0	1	0.73	0.75	0.62	0.65	0.7	0.69	3	41
1	0	0	1	0	0	0	0	1	0.74	0.75	0.62	0.65	0.7	0.692	3	42
1	0	0	1	0	0	0	0	1	0.73	0.75	0.61	0.64	0.7	0.686	3	43
0	0	1	0	0	0	0	1	0	0.8	0.78	0.73	0.72	0.75	0.756	3	44*
1	1	0	0	0	0	0	0	0	0.7	0.63	0.65	0.68	0.72	0.676	2	45
1	0	1	0	0	0	0	0	0	0.69	0.63	0.64	0.68	0.71	0.67	2	46
1	0	0	1	0	0	0	0	0	0.43	0.52	0.29	0.28	0.3	0.364	2	47
1	0	0	0	0	0	0	1	0	0.34	0.43	0.21	0.2	0.2	0.276	2	48
1	0	0	0	0	0	0	0	1	0.51	0.59	0.36	0.36	0.38	0.44	2	49
0	0	1	0	0	0	1	0	0	0.71	0.76	0.68	0.71	0.74	0.72	2	50*
0	0	1	0	0	0	0	0	0	0.7	0.64	0.68	0.68	0.72	0.684	1	51*